NASA TECHNICAL MEMORANDUM

NASA TM X- 62,318

NASA TM X- 62,318

AIRFOIL WAKE VORTEX CHARACTERISTICS IN THE FAR FIELD

K. L. Orloff, D. L. Ciffone, and D. Lorincz

Ames Research Center
Moffett Field, Calif. 94035

November 1973

NOMENCLATURE

a	vortex core radius
AR	aspect ratio
b	wing span
c	wing reference chord
C_L	lift coefficient
f_z	particle scattering frequency, vertical component
f_x	particle scattering frequency, horizontal component
r	radial distance from vortex core centerline
t	test time, referenced to passage of towing strut at test section
u	velocity component along the x axis
U_∞	towing velocity
V_θ	vortex tangential velocity component
V_x	vortex axial velocity component
w	velocity component normal to the x axis
X	downstream ordinate, aft from trailing edge at wing tip
α	angle of attack (referenced to wing root chord)
θ	intersection angle of the crossed laser beams
Δ	wing sweep angle
λ	wing taper ratio
Γ_0	total measured circulation from one vortex (from measurement)
μ	index of refraction

AIRFOIL WAKE VORTEX CHARACTERISTICS IN THE FAR FIELD

K. L. Orloff, D. L. Ciffone, and D. Lorincz*

Ames Research Center

ABSTRACT

Tangential and axial velocity profiles have been measured in the far-field wake vortices of several different airfoils. The results are summarized and discussed. A scanning laser velocimeter was used at the University of California's water tow-tank facility at Richmond, California, to obtain data up to 10^3 chord lengths (approximately 200 span lengths) behind airfoils with rectangular, diamond-shaped, and swept-wing planforms at several different angles of attack. The results show general agreement with wind-tunnel measurements made in the near field. The results identify two separate flow regions for the dependence of vortex maximum tangential velocity on downstream distance; an inviscid region where the velocity remains constant after rollup to downstream distances of 200 chord lengths, and then a decay or viscous region that persisted to the limit of the test distance. The decay rates appear to be sensitive to both angle of attack and span loading. The maximum tangential velocity for downstream distances to 40 span lengths was reduced by a factor of 2 by changing from an elliptic (swept wing) or rectangular span loading to a triangular-like span loading (diamond-shaped planform wing). Measured axial velocity defects are shown to agree with those predicted by laminar theory.

INTRODUCTION

The purpose of the present investigation was (1) to measure the far wake vortex velocity distributions generated by airfoils being towed through a water tow-tank, (2) to compare these results with near wake data obtained in air in wind tunnels with similar airfoils, and (3) to investigate the effects of angle of attack and span loading due to wing planform on the far wake characteristics.

The investigation was performed in the University of California's water towing-tank facility at Richmond, California. Test Reynolds number based on wing chord was nominally 2.43×10^5. Velocity distributions in the far wakes of rectangular, triangular, and swept-wing planforms were measured with the laser velocimeter instrument discussed in references 1 to 3. In an attempt to separate pure span loading effects from turbulence effects, simple wing planforms were used to obtain different span load distributions as opposed to the use of deflected surfaces with one common planform. The effects of angle of attack as well as span loading were investigated at downstream distances to 10^3 chord lengths (or 200 spans).

---

*Summer student at Ames Research Center from California Polytechnic Institute, San Luis Obispo, California.

The results are compared with previous near-field, wind-tunnel measurements (refs. 2–4), with far-field results obtained in flight (ref. 5), and with water tow-tank results using the hydrogen bubble technique (ref. 6).

EXPERIMENTAL APPARATUS AND PROCEDURE

The test facility was the University of California's water tow-tank located in Richmond, California. The tank is 61 m long, 2.44 m wide, and 1.7 m deep (fig. 1). However, only 35 m of the length were used. The test section was positioned approximately 14 m from the starting point of the carriage and 21 m from the stopping location (fig. 1). Large glass windows at the test section extend from a point approximately 0.6 m above the bottom of the tank to well above the free surface. The carriage, from which the models and connecting strut were suspended, is electrically driven and is capable of a maximum speed of just over 2 m/sec. A photosensitive timing system mounted on the carriage structure measures the speed of the carriage.

The length of the streamlined strut to which the models were mounted was such that the trailing edge of the airfoil was 0.7 m above the bottom of the tank (1 m from the free surface). This strut was centered on the carriage and hence alined with the center of the tank. Angles of attack of 4°, 5°, and 8° were available using wedge blocks inserted at the attachment point at the top of the strut. In addition, the airfoils were installed in an inverted position so that the vortex pair would rise toward the free surface as they aged, allowing better visualization.

Three separate airfoil planforms were investigated (fig. 2). The rectangular and swept configurations were selected because the vortices on these configurations had previously been measured with a laser velocimeter in the Ames 7- by 10-Foot Wind Tunnel (refs. 2 and 3) and with a rotating hot wire anemometer in the 40- by 80-Foot Wind Tunnel (ref. 4). Data have also been previously obtained on rectangular planforms from vortex studies in water tow-tanks (refs. 6 and 8). The diamond-shaped wing (triangular span loading) was included because Betz (ref. 9) calculations by Rossow (ref. 10) indicated that triangular span loadings would yield low wake rotational velocities. The pertinent geometric characteristics of each wing are presented in figure 2. The swept-wing planform is cambered over the outer 2/3 of the span.

To mark the vortex centerline, a thin sheet of air bubbles was generated across the tank approximately 1.5 m upstream (toward the starting end) of the test section location of the laser. The axial velocity defect in the vortex core region then acted in such a way as to drag some of these bubbles toward the passing airfoil; the radial pressure gradient associated with the rotational flow centered the bubbles in single file, producing a fine string of bubbles along the vortex centerline. As the vortex pair rose in the tank, the laser system was raised manually to maintain the optical axis aligned with the vortex centerline. Spanwise continuous traversals of the focal point through the vortex were then made with an automatic scan reversal set to encompass the area of interest (i.e., the near vortex and a substantial region on either side of its core). Polystyrene copolymer latex solution was added to the water in the region of the test section to ensure that a sufficient number of scattering particles would be present. The size of these particles was between 2 and 15 μ.

The timing for a given run began when the streamlined strut passed through the outgoing laser light at the test station. Several runs were made with test times greater than 50 sec after passage of the model or, equivalently (for $U_\infty = 2.07$ m/sec), at downstream distances of 1000 chord lengths. For run times up to 50 sec, the vortex pair maintained a reasonable rise rate toward the free surface with little drift toward the side walls of the tank.

DATA REDUCTION AND PRESENTATION

Rapid spatial scanning of the trailing vortex flow was accomplished with a two-dimensional laser velocimeter system. Use of this two-color (four-beam) technique allowed the axial and tangential velocities to be measured simultaneously during the time a vortex was being traversed spatially. Measured frequencies are linearly related to the orthogonal velocity components by the following equations:

$$u = \frac{(5145\ \text{Å})}{2\mu} \frac{f_x}{\sin \theta/2}$$

$$w = \frac{(4880\ \text{Å})}{2\mu} \frac{f_z}{\sin \theta/2}$$

where x and z refer to horizontal and vertical values, respectively. These expressions accurately represent the vortex flow field when a centerline penetration of the vortex is made, then $u = V_x$ and $w = V_\theta$, the axial and tangential velocities, respectively. The angular dependence, $\sin \theta/2$, is a function of the distance of the crosspoint from the transmitting lens. The velocimeter was hoisted vertically so that the aging vortices could be tracked as they rose in the tank. The index of refraction for water is $\mu = 1.33$.

Signal processing was accomplished with two identical spectrum analyzer systems. The vertical (signal energy content) and horizontal (frequency position) outputs of each analyzer were recorded on magnetic tape. Selected traversals could then be transferred to oscillograph paper. Voltages from linear potentiometers, one driven by the scanning lens carriage and the other by the laser hoist carriage, were also recorded. These voltages (representing the tank location of the test point) and the frequency information from the spectrum analyzer were processed to yield velocity and spatial position relative to the wing trailing edge.

Vortex maximum velocities are presented as fractions of towing speed, U_∞, and location, X, relative to the wing tip trailing edge ($X = 0$), normalized to either wing reference chord, c, or span, b. Velocity distributions normalized on towing speed are presented as functions of percent wing span, b, for various downstream distances, X/b. Maximum tangential velocities represent an average of the inboard and outboard peak tangential velocity from a given velocity distribution.

RESULTS AND DISCUSSION

A summary of vortex maximum tangential velocity as a function of downstream distance for the rectangular wing at angles of attack of 4°, 5°, and 8° is presented in figure 3. The towing speed was 2.07 m/sec. Also shown in the figure, for comparison, are the results obtained in the Ames 7- by 10-Foot and 40- by 80-Foot Wind Tunnels (refs. 2 and 4). Both the 7- by 10-Foot Wind Tunnel laser results at 2 chord lengths and the 40- by 80-Foot Wind Tunnel hot-wire data at 53 and 165 chord lengths are in reasonably good agreement with the tow-tank results at the same lift coefficients. The water tow-tank results (ref. 6) obtained with a hydrogen bubble technique are also shown for comparison. The short dashed line represents data at 4° and 8° angle of attack at towing speeds of 1 to 4 m/sec. Although the velocity decay rate is comparable to the present test results, the measured values of velocity are lower and are probably associated with inaccuracies in data reduction using the hydrogen bubble technique.

In addition to laboratory experiments, the flight-test data of reference 5 are presented for comparison in the far field. The flight-test Reynolds number is a factor of 20 greater than the water-tank data, and the flight-test lift coefficient is slightly higher. These results indicate general agreement in maximum velocity levels but show a lower rate of decay.

The present data identify two separate flow regions: a plateau or inviscid region where the maximum rotational velocity remains constant after rollup to downstream distances of approximately 200 chord lengths, and a decay or viscous region that persists to the limits of the test distance, about 10^3 chord lengths. The velocity decays inversely with downstream distance at something less than the 2/3 power at 8° angle of attack and like the square root power at the lower angles of attack.

There was concern whether the initiation of the velocity decay was a real flow phenomenon or a consequence of starting and stopping the model. The vertical arrows in figure 3 indicate the earliest time that a starting or stopping wave disturbance could be expected to alter the test results. The times indicated are related to a starting wave that propagates at a speed equal to the maximum tangential velocity. This is the most conservative estimate of the appearance of a motion wave; in reality, these disturbances should appear considerably later (ref. 11). However, there was no evidence that either a starting or stopping wave was disturbing the vortex, at least for test times attained in this experiment ($t = 50$ sec). Neither visual nor measured perturbations in vortex core size nor axial velocity indicated the passage of a disturbance wave. This conclusion was checked qualtitatively by stopping the carriage at different distances beyond the test section and visually observing the bubble movement along the vortex core centerline at the test section. At a towing speed of 2 m/sec and a carriage stopping distance greater than 10 m beyond the test station, there was no indication of a stopping wave moving through the test section for the duration of the data-gathering period. For all test runs, the carriage was stopped 21 m beyond the test section. It seems safe to conclude that the onset of velocity decay at about 100 chord lengths is not related to starting or stopping the model.

Also shown in the figure is the time after the model passed through the test section and the related downstream distance behind a typical, wide-body, jet transport. Within the scatter of the data at distances of 10^3 chord lengths (approximately 6.44 km behind a typical wide-body jet), the effect of angle of attack on the generating aircraft is not readily distinguishable in the wake velocities.

Figure 4 shows how the maximum vortex core axial velocity (in the towing direction) for the rectangular wing decreases with downstream distance and angle of attack. The wind-tunnel data of references 2 and 4 and the water-tank data of references 6 and 8 are shown for comparison. The present data indicate a far-field maximum axial velocity decay that is inversely proportional to downstream distance to approximately 1/4 power. Also shown in the figure are the axial velocity defect and rate of decay on the vortex centerline as computed from the laminar theory of reference 7; the comparison is remarkably good.

A comparison of the rectangular wing axial velocity profiles measured at different test times is presented in figure 5. These results characterize the radial diffusion of the axial velocity defect. A profile obtained in the near-field, laser velocimeter, wind-tunnel experiment (ref. 2) at $x/c = 2.0$ ($t = 0.1$ sec) is included to emphasize the extent to which the momentum is initially concentrated. To conserve linear momentum during this diffusion process, the first moment of the area beneath each curve should remain constant with time. However, since a significant percentage of the linear momentum is contained near the outer edges of the defect region, an accurate calculation of the total linear momentum is hindered by uncertainties in measuring the near-zero velocities in this region. Nevertheless, the diffusive nature of the axial structure is clearly documented and, from fairings such as these, the core velocity along the axis can be extracted and its subsequent decay considered.

The growth of the core radius with downstream distance is presented in figure 6. The line through the 8° data points indicates that the growth of the core is essentially proportional to downstream distance, whereas the growth rate of the 4° data shows a proportionality somewhere between a square root and a 2/3 dependence. The water-tank data of reference 6 and the flight data of reference 5 are shown for comparison. While the growth rates are comparable, the magnitudes of the water-tank data (ref. 6) are somewhat higher than those of this experiment, while the flight data are lower. Hot-wire, wind-tunnel results (ref. 4) generally agree well with present data.

The effects of downstream distance and span loading on maximum tangential velocity are compared in figure 7. The measured circulations for the three planforms are also listed. Of particular significance is the fact that, although the measured circulation of the diamond-shaped planform wing is comparable to that of the swept-wing planform, its maximum rotational velocity is lower by a factor of 2. This fact is consistent with the theoretical calculations of Rossow (ref. 10) as presented in figure 8. It is a pure span loading effect that results from the reduced vorticity shed near the tip of the diamond-shaped wing. Another significant result seen in figure 7 is that, although this factor of 2 in rotational velocity is evident in the near field, at 200 span lengths or greater the effects of span loading on velocity are not readily distinguishable within the scatter of the data. The decay rate appears to be sensitive to span loading. The inviscid or "plateau" region extends to downstream distances of ~35 span lengths for the swept and rectangular planforms as compared to ~80 span lengths for the diamond-shaped planform.

Figure 9 compares the complete tangential velocity profile for each wing planform as measured at 20 span lengths where, according to figure 7, the measured rotational velocities are insensitive to downstream distance. Hence, differences in the velocity profiles result from differences in span loading and/or circulation, but not turbulent decay. The triangular span loading yields a lower concentration of vorticity in the core and diminished circumferential velocities in the adjacent regions. Both features are desirable in alleviating the wake vortex hazard.

At 100 span lengths downstream, in the viscous flow region, the velocity profiles are quite similar (fig. 10), and any dependence on generating planform span loading is no longer distinguishable within the scatter of the data. The rectangular and swept-wing planforms have decayed to the levels of the triangular loading at this downstream distance. The tangential velocities associated with the diamond-shaped planform (triangular-like span loading) decay very little with downstream distance (as illustrated in fig. 11).

CONCLUSIONS

It has been shown that a laser velocimeter can be used in conjunction with a water tow-tank to measure trailing vortex characteristics. The results obtained are shown to be in relatively good agreement with near-field results obtained in wind tunnels on similar models, which adds credibility to wake vortex data obtained in both facilities. The results identify two separate flow regions for the dependence of vortex maximum tangential velocity on downstream distance: an inviscid region where the velocity remains constant after rollup to downstream distances of approximately 200 chord lengths, and then a decay or viscous region that persists to the limit of the test distance. The decay rates appear to be sensitive to both angle of attack and span loading. For downstream distances up to 40 span lengths, a factor of 2 reduction in maximum tangential velocity is obtained by changing from an elliptic (swept wing) or rectangular span loading to a triangular-like span loading (diamond-shaped planform wing). However, it appears that neither angle of attack nor variations in span loading due to the changes in wing planform are effective in influencing the maximum tangential vortex velocity at distances 5 miles or greater behind a typical wide-body jet. Good agreement has been shown between both measured axial velocity defects and decay rates and those predicted from the laminar theory of Moore and Saffman (ref. 7). It remains to be seen whether flap and/or spoiler deflections, which introduce turbulence into the wake while altering the span loading, will yield the same results.

REFERENCES

1. Grant, G. R.; and Orloff, K. L.: A Two-Color, Dual Beam Backscatter Laser Doppler Velocimeter. NASA TM X-62,254, 1973.

2. Orloff, K. L.; and Grant, G. R.: The Application of a Laser Doppler Velocimeter to Trailing Vortex Definition and Alleviation. NASA TM X-62,243, 1973.

3. Ciffone, D. L.; Orloff, K. L.; and Grant, G. R.: Laser Doppler Velocimeter Investigation of Trailing Vortices Behind a Semispan Swept Wing in a Landing Configuration. NASA TM X-62,294, 1973.

4. Corsiglia, V. R.; Schwind, R. G.; and Chigier, N. A.: Rapid Scanning, Three-Dimensional, Hot-Wire Anemometer Surveys for Wing Tip Vortices. J. Aircraft, vol. 10, no. 12, 1973, pp. 752–757.

5. McCormick, B. W.; Tangler, J. L.; and Sherrieb, H. E.: Structure of Trailing Vortices. J. Aircraft, vol. 5, no. 3, 1966, pp. 260–267.

6. Lezius, D. K.: Study of the Far Wake Vortex Field Generated by a Rectangular Airfoil in a Water Tank. NASA TM X-62,274, 1973.

7. Moore, D. W.; and Saffman, P. G.: Axial Flow in Laminar Trailing Vortices. Proc. Roy. Soc. London A, vol. 333, 1973, pp. 491–508.

8. Olsen, J. H.: Results of Trailing Vortex Studies in a Towing Tank, in Aircraft Wake Turbulence and Its Detection, edited by J. H. Olsen, A. Goldburg, and M. Rogers, Plenum Press, New York, 1971, pp. 455–472.

9. Betz, A.: Behavior of Vortex Systems. NACA TM 713, 1933.

10. Rossow, V. J.: On the Inviscid Rolled-Up Structure of Lift Generated Vortices. J. Aircraft, vol. 10, no. 11, 1973, pp. 647–650.

11. Brown, C. E.: The Use of Ship Model Basins for the Study of Vortex Wake Phenomena. Tech. Rept. 7115-2, Hydronautics, Inc., March 1973.

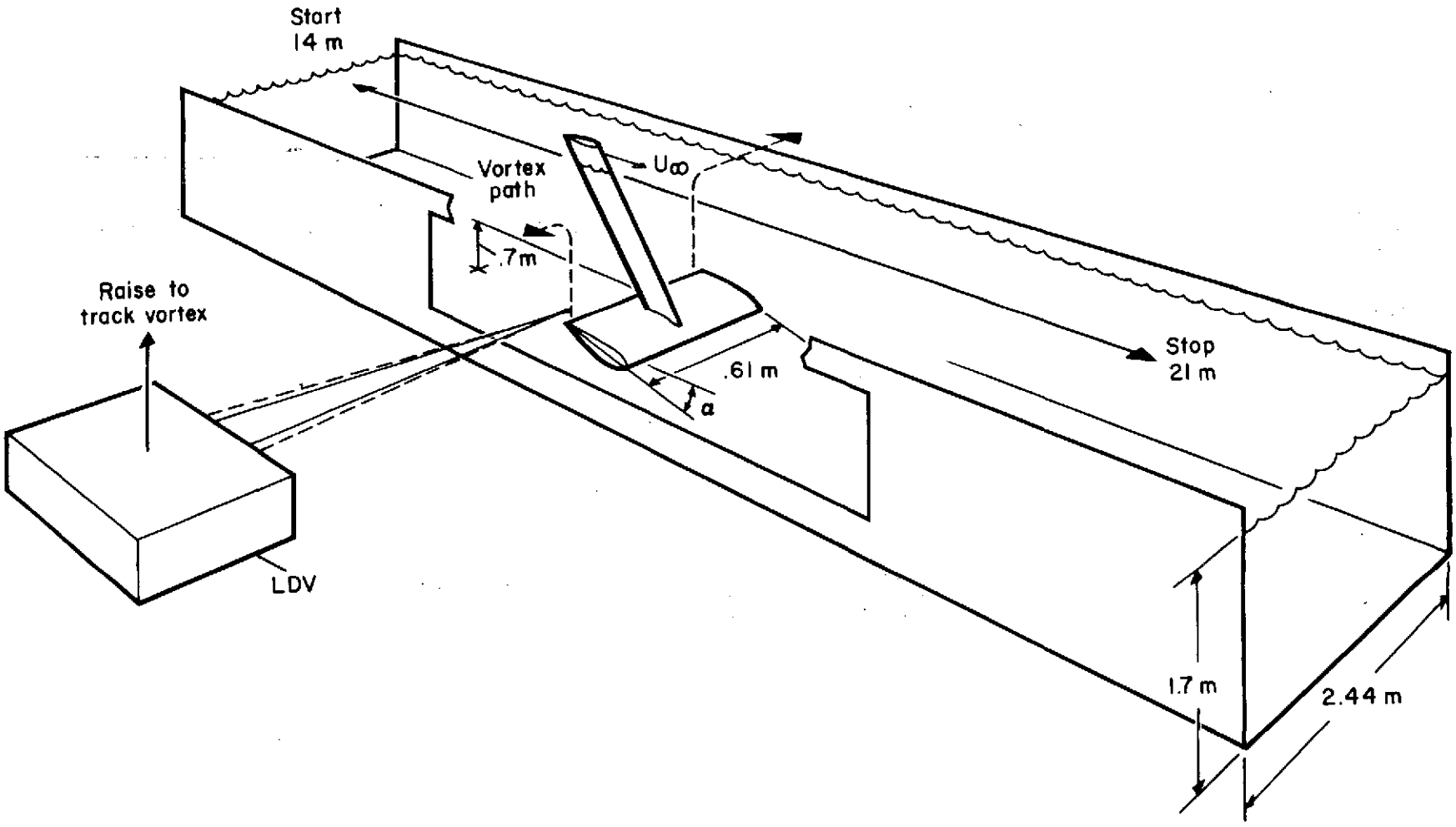

Figure 1.– Tow-tank, model installation, and vortex-tracking technique.

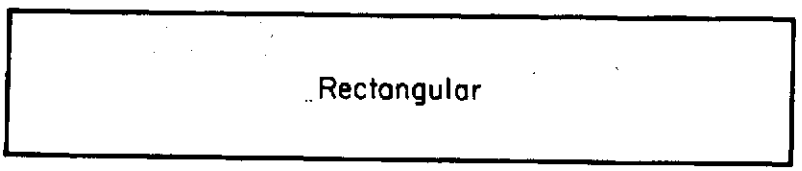

C = .114 m (4.5 in.)
AR = 5.33
NACA 0015 airfoil

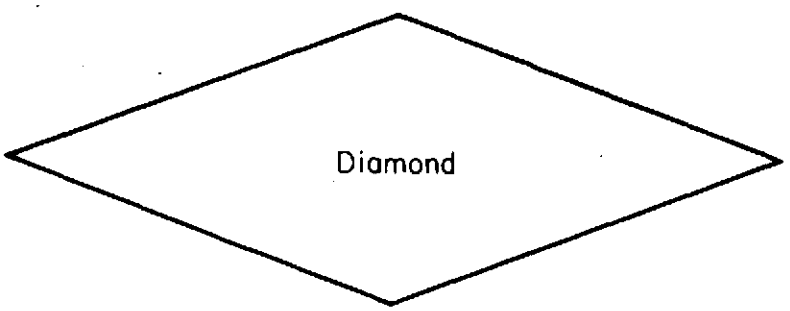

C = .114 m (4.5 in.)
AR = 5.33
C_{ℓ} = .228 m (9.0 in.)
NACA 0015 airfoil

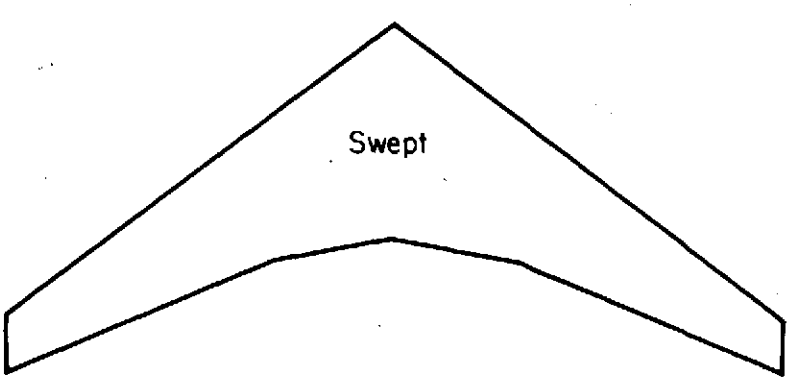

C = .104 m (4.1 in.)
AR = 5.85
Λ = 38.6°
λ = .25

Figure 2.– Wing planforms to obtain different span load distributions, b = 0.61 m (2 ft).

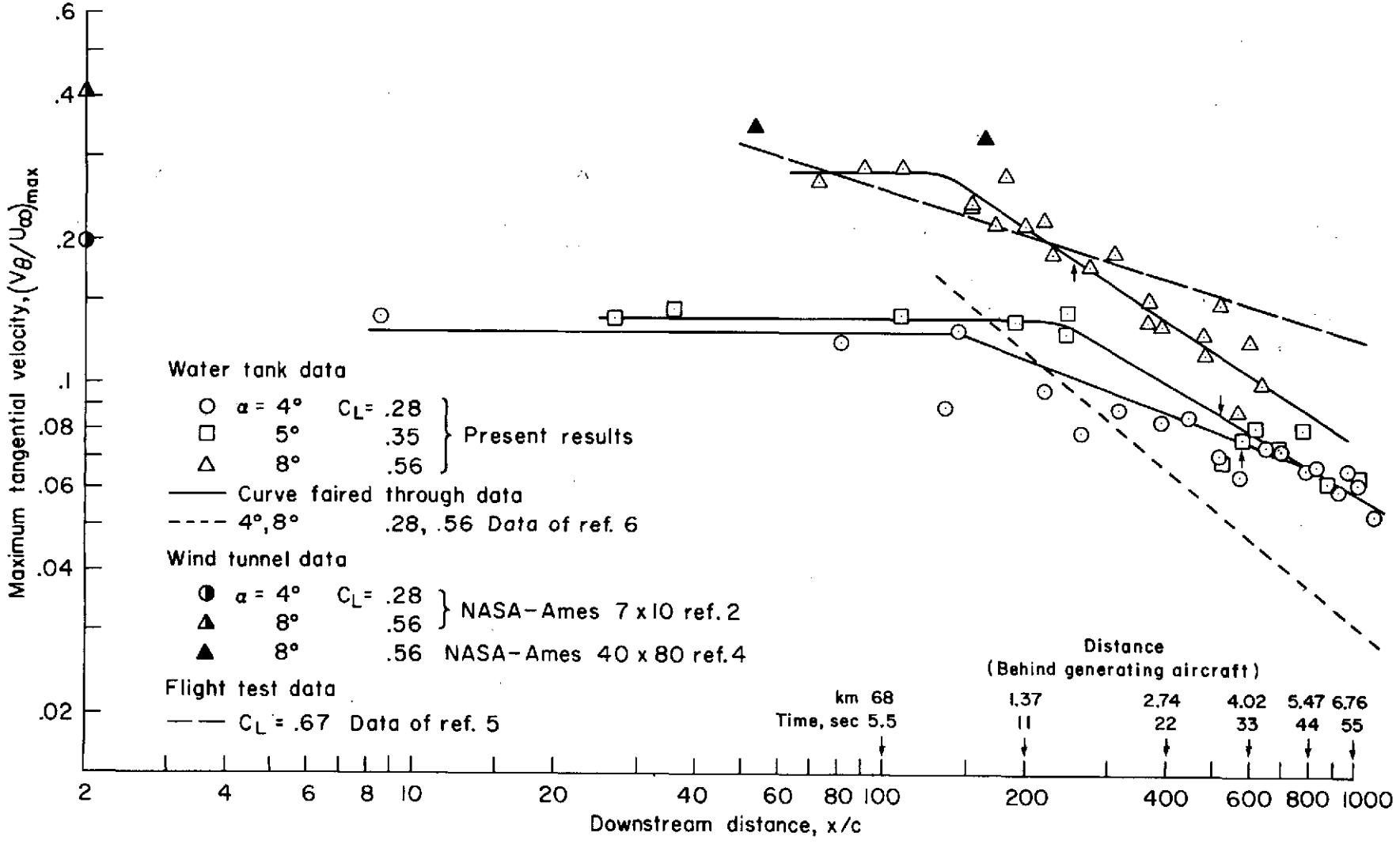

Figure 3.– Dependence of maximum tangential velocity on downstream distance – rectangular planform; U_∞ = 2.07 m/sec.

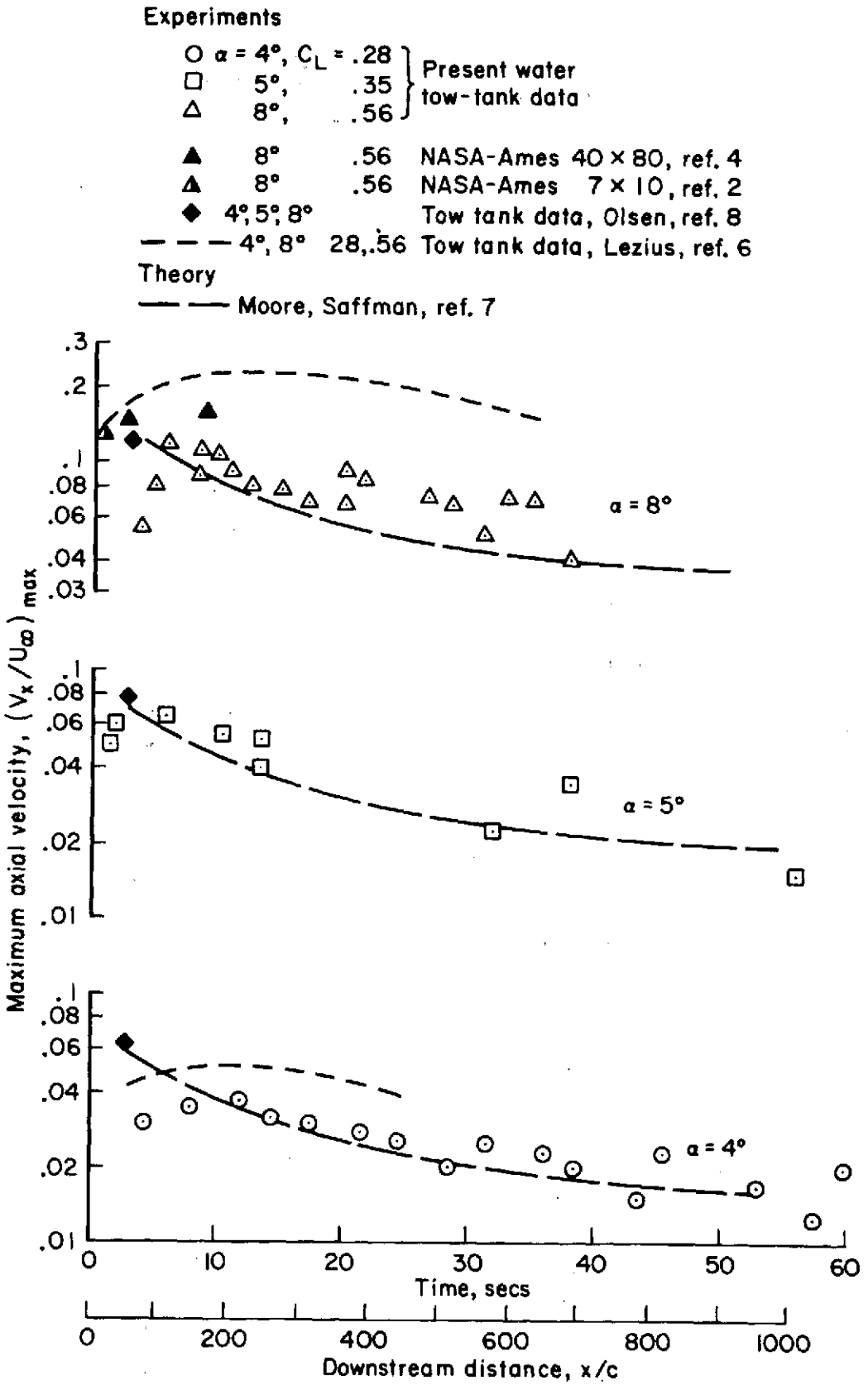

Figure 4.– Dependence of maximum axial velocity (defect along vortex centerline) on downstream distance – rectangular planform; $U_\infty = 2.07$ m/sec.

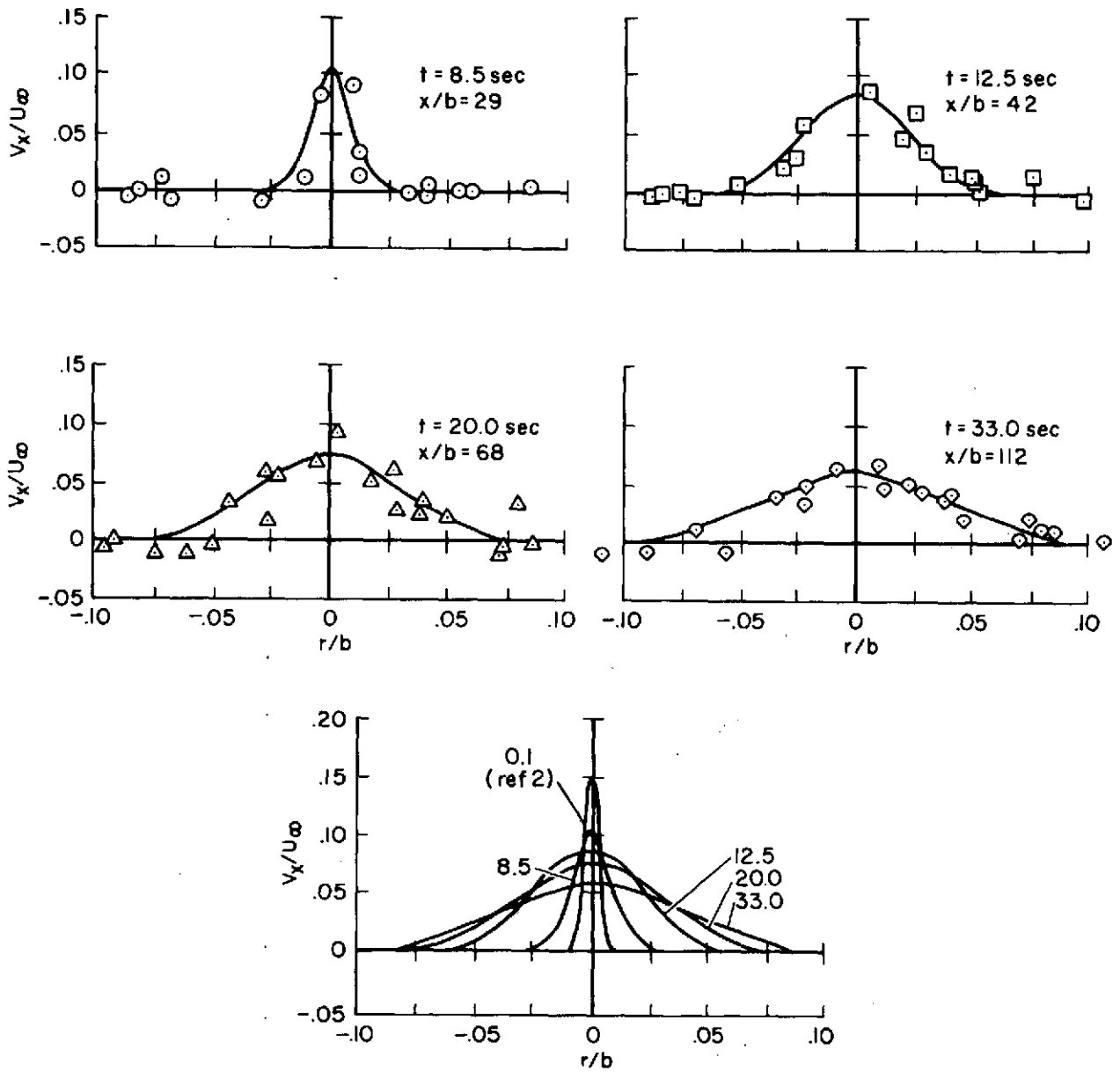

Figure 5.– Radial distribution of axial velocity illustrating the diffusive nature of the core defect region as the vortex ages – rectangular planform; U_∞ = 2.07 m/sec, $\alpha = 8°$, $C_L = 0.56$.

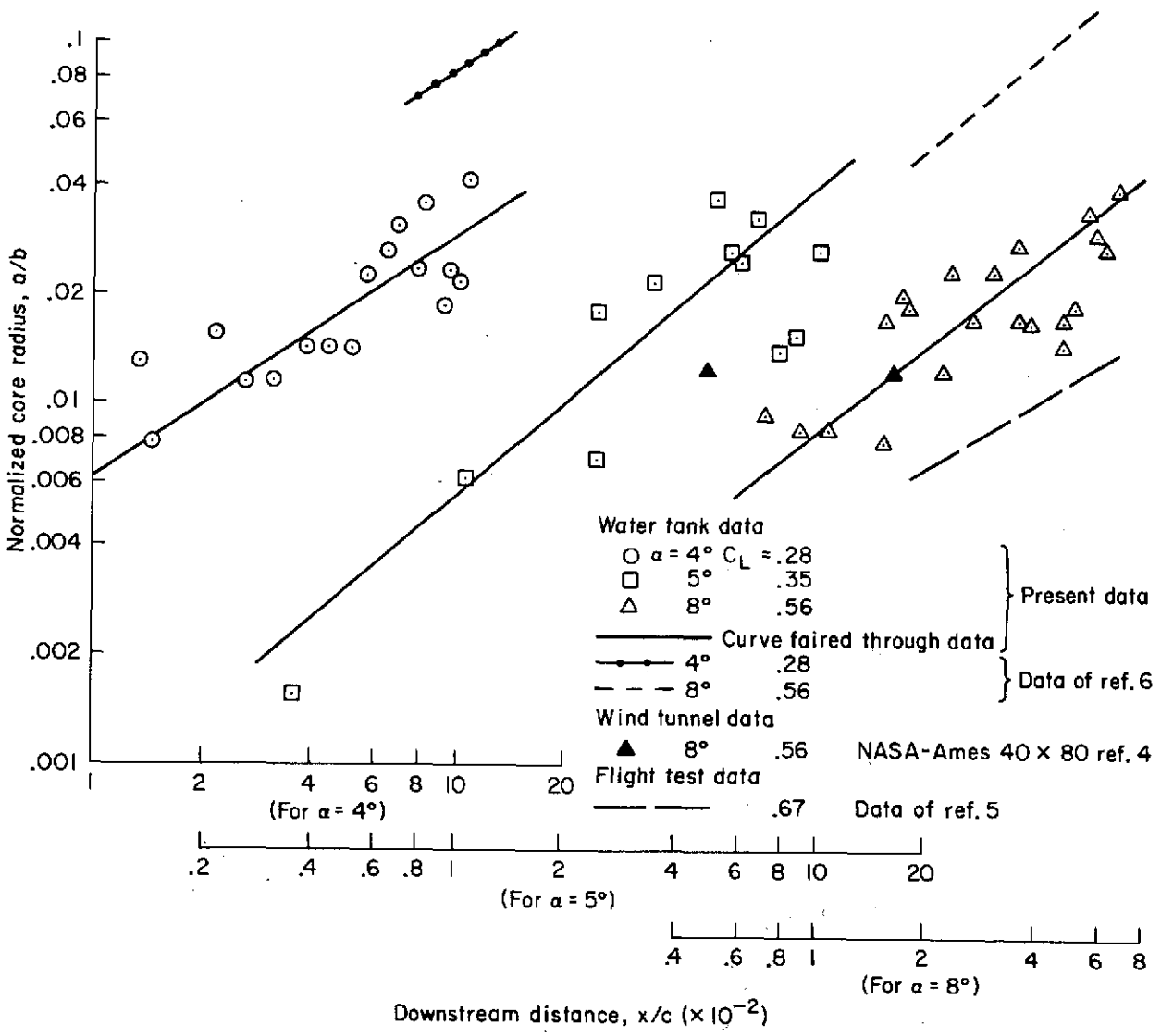

Figure 6.– Growth of vortex core radius with downstream distance – rectangular planform; $U_\infty = 2.07$ m/sec.

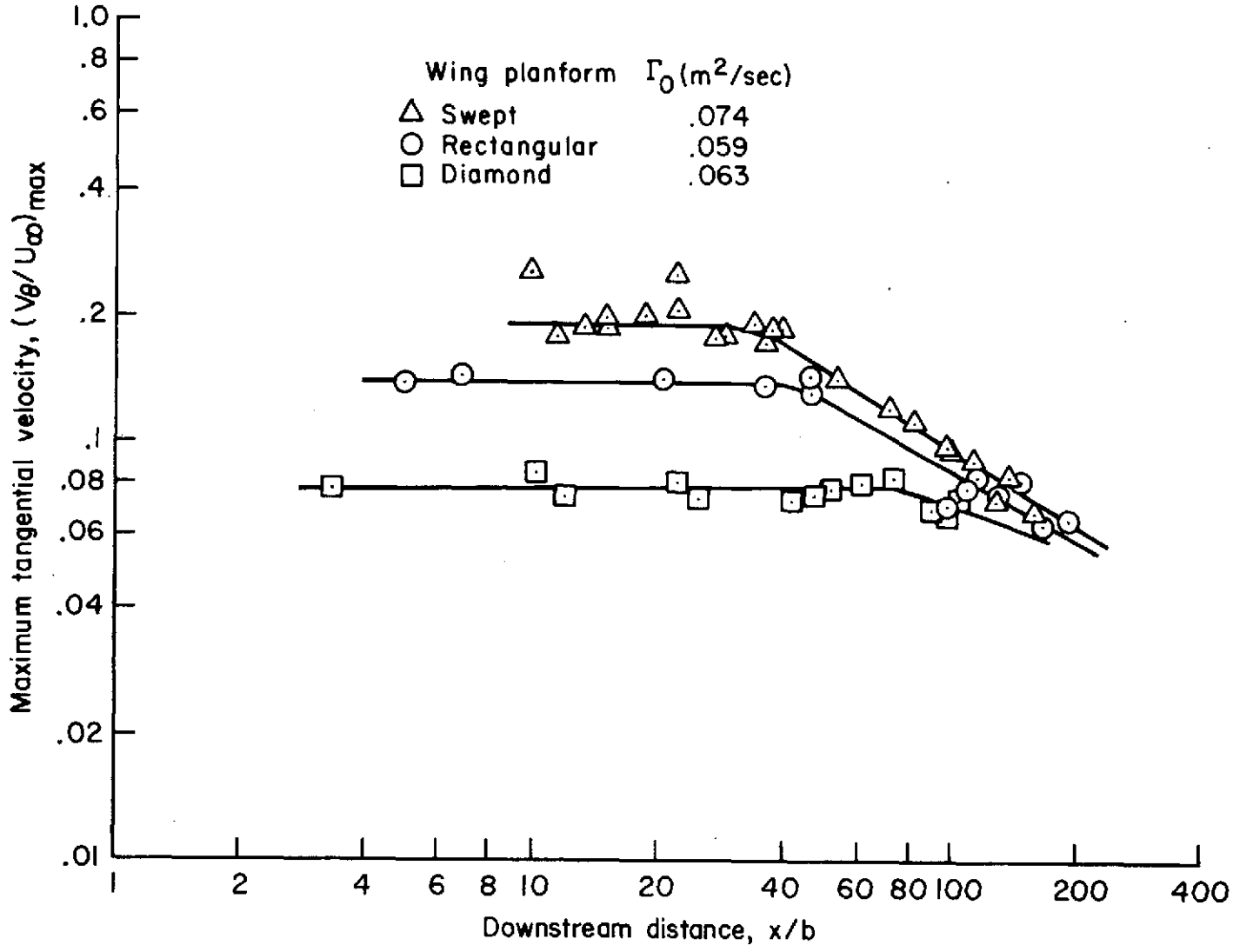

Figure 7.– Effect of span loading on downstream vortex characteristics; $\alpha = 5°$, $U_\infty = 2.07$ m/sec.

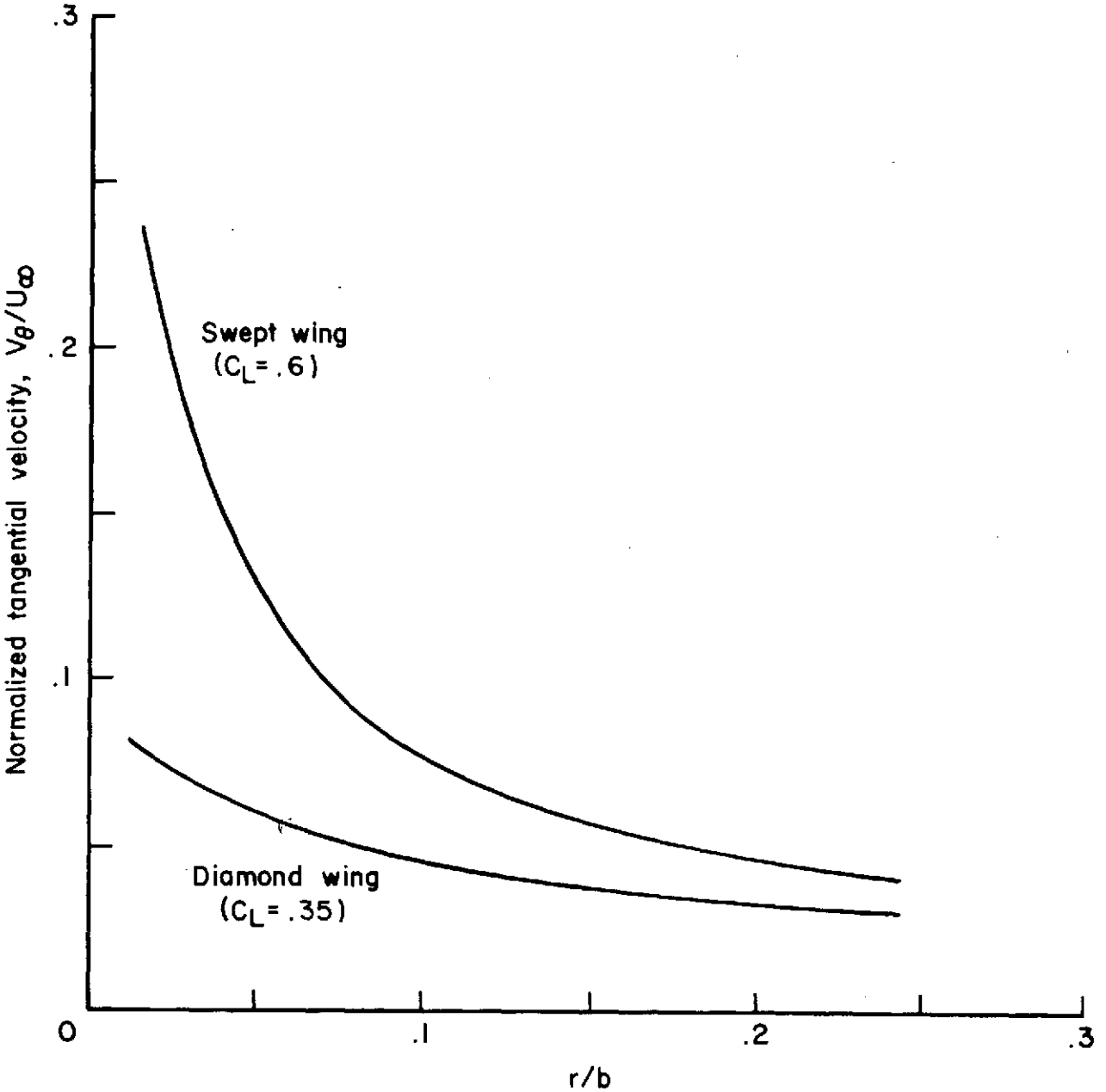

Figure 8.– Theoretically predicted tangential velocity profiles obtained from Rossow's (ref. 10) modified Betz technique; $U_\infty = 2.07$ m/sec, $\alpha = 5°$.

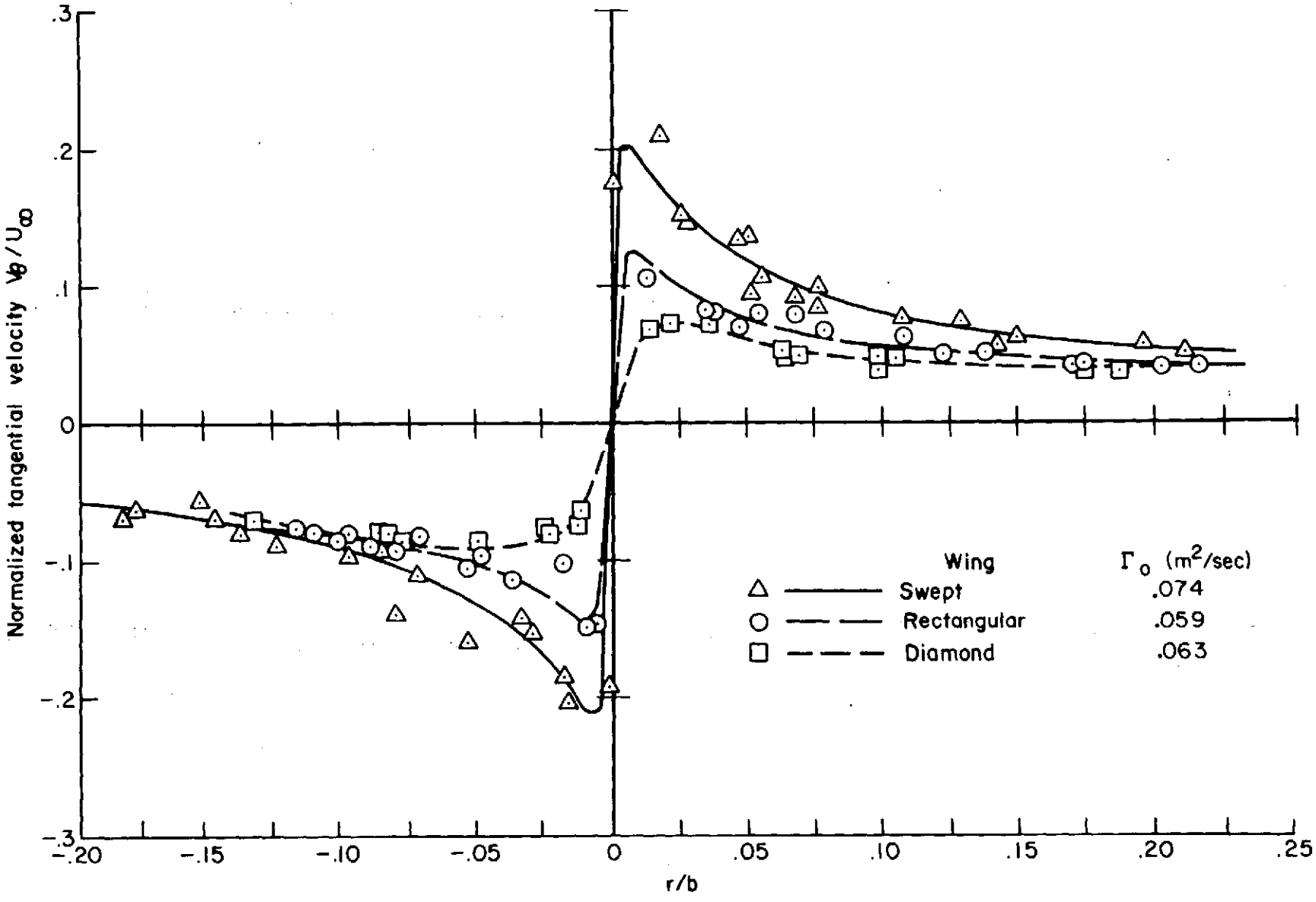

Figure 9.– Radial distribution of tangential velocity for different wing planforms at X/b = 20; $\alpha = 5°$, $U_\infty = 2.07$ m/sec.

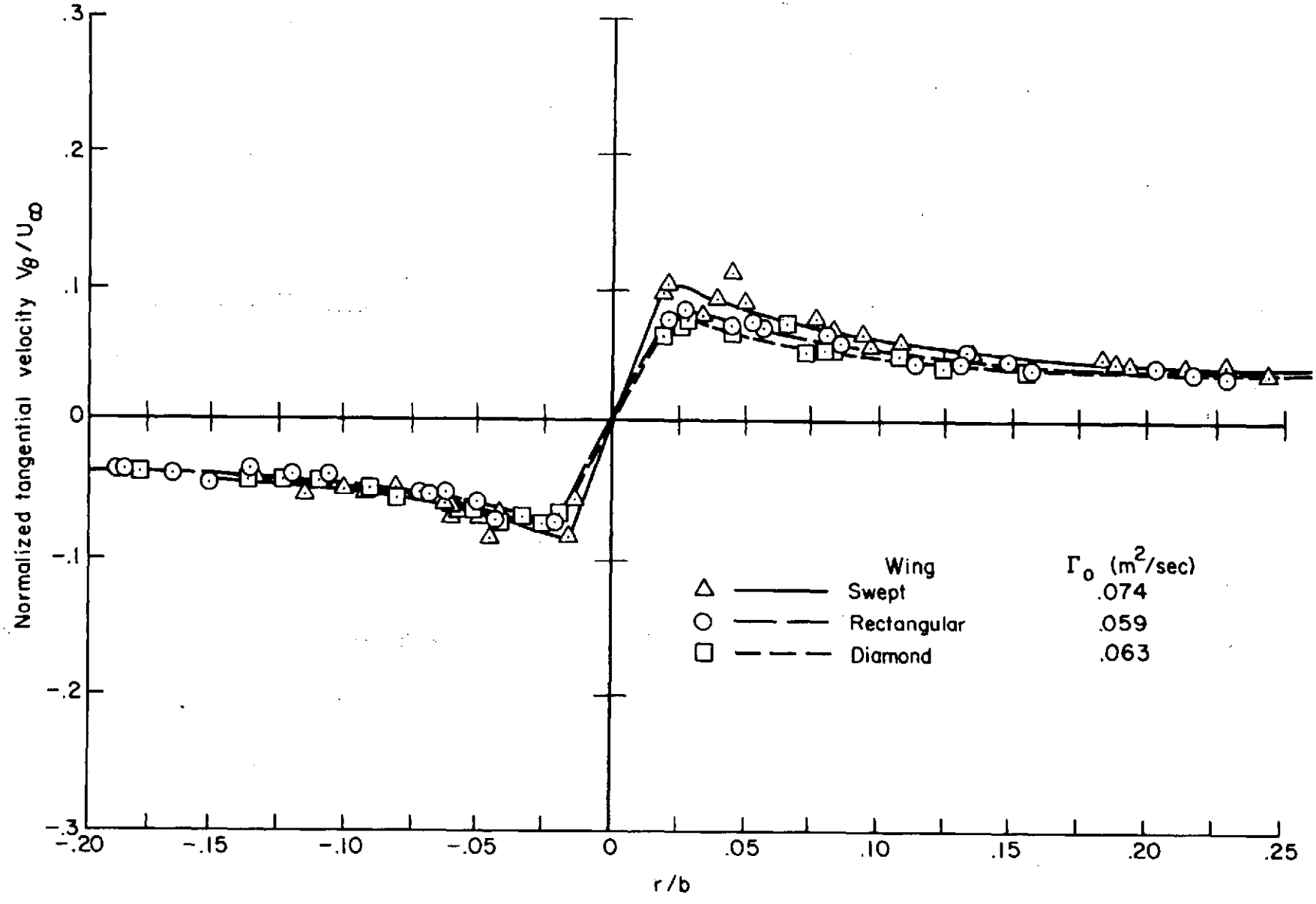

Figure 10.– Radial distribution of tangential velocity for different wing planforms at X/b = 100; $\alpha = 5°$, $U_\infty = 2.07$ m/sec.

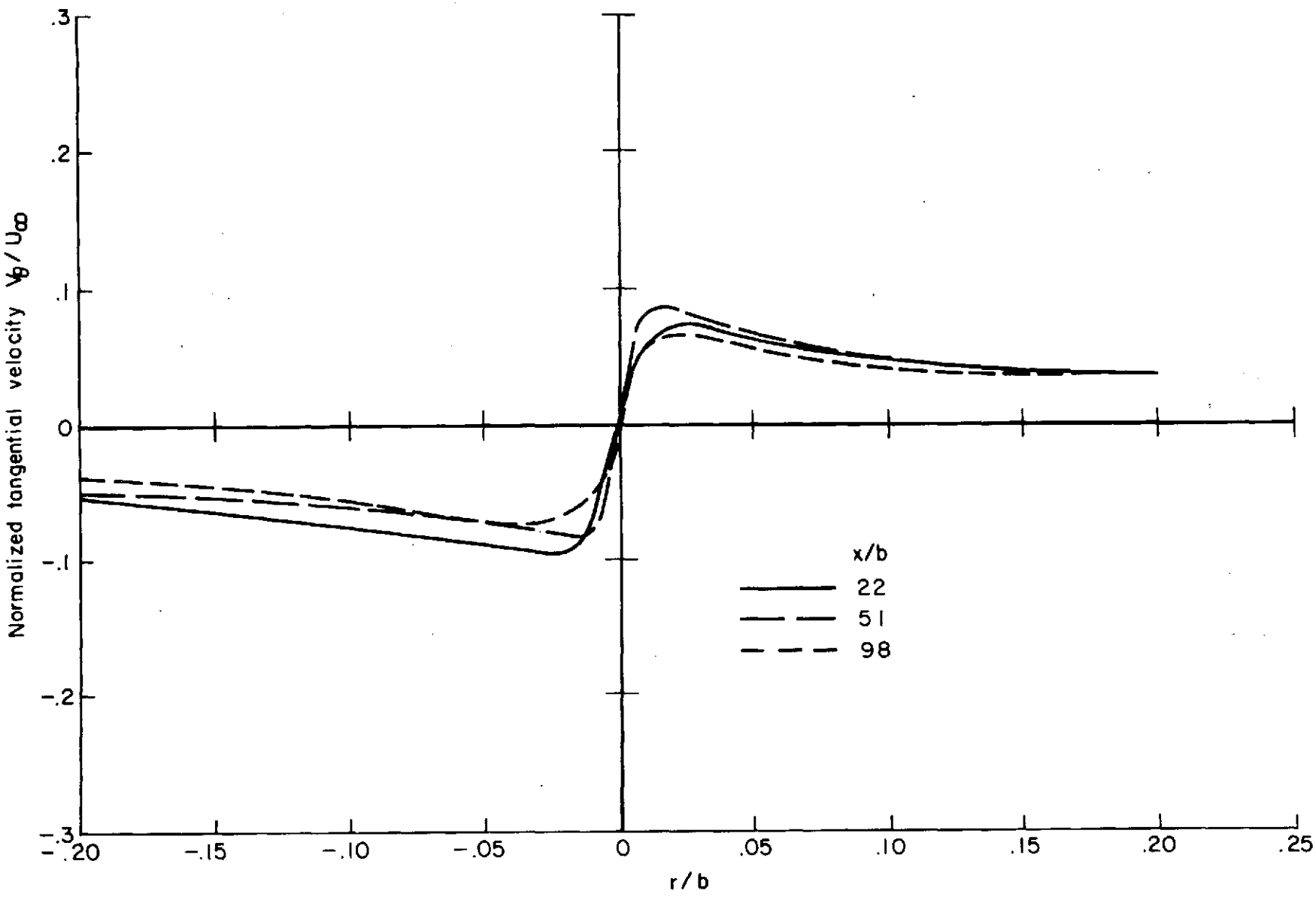

Figure 11.– Invariance of tangential velocity profile for triangular loading to downstream distance; $\alpha = 5°$, $U_\infty = 2.07$ m/sec.